REPORT DOC

AD-A236 924

Form Approved
OMB No. 0704-0188

Public reporting burden for this collection of information is estim
maintaining the data needed, and comp ting and reviewing the co
suggestions for reducing this burden, to Washington Headquarters
and to the Office of Management and Budget, Paperwork Reduction Project
ions, searching existing data sources, gathering and
other aspect of this collection of information, including
Davis Highway, Suite 1204, Arlington, VA 22202-4302

1 AGENCY USE ONLY (Leave blank)	2 REPORT DATE	3 REPORT TYPE AND DATES COVERED
	May 1991	Professional Paper

4 TITLE AND SUBTITLE

EIGENVALUES OF COVARIANCE MATRIX FOR TWO-SOURCE ARRAY PROCESSING

5 FUNDING NUMBERS

PR: SXB2
WU: ICSXB200
PE: 0602111N

6 AUTHOR(S)

S. I. Chou

7 PERFORMING ORGANIZATION NAME(S) AND ADDRESS(ES)

Naval Ocean Systems Center
San Diego, CA 92152-5000

8 PERFORMING ORGANIZATION REPORT NUMBER

9 SPONSORING/MONITORING AGENCY NAME(S) AND ADDRESS(ES)

Naval Ocean Systems Center
Block Programs
San Diego, CA 92152-5000

10 SPONSORING/MONITORING AGENCY REPORT NUMBER

11 SUPPLEMENTARY NOTES

12a DISTRIBUTION/AVAILABILITY STATEMENT

Approved for public release; distribution is unlimited.

12b DISTRIBUTION CODE

A-1

13 ABSTRACT (Maximum 200 words)

Eigenvalue weighting appears in some noise subspace methods, in parametric signal subspace fitting methods, and in nonparametric subspace adaptive nulling beamforming. For a two-source array processing scenario, normalized eigenvalues' expressions λ_1 and λ_2 are reduced to forms depending only on a real triplet: phase-dependent variable ξ, phase-independent variable η, and power ratio $\frac{\pi_1}{\pi_2}$. (ξ, η) is confined to an isosceles-like region. We characterize:

- this isosceles-like region and the many-to-one mapping from the Cartesian product of the temporal and spatial correlation unit-disks onto this region, and
- the behavior of the eigenvalues and their ratio as functions of the real triplet both analytically and graphically with respect to array processing.

Published in *Proceedings of the 24th Annual Asilomar Conference on Signals, Systems, and Computers*, Nov 1990.

14 SUBJECT TERMS		15 NUMBER OF PAGES
tracker/correlator	ultra wideband radar	
dim target	HFDF	16 PRICE CODE

17 SECURITY CLASSIFICATION OF REPORT	18 SECURITY CLASSIFICATION OF THIS PAGE	19 SECURITY CLASSIFICATION OF ABSTRACT	20 LIMITATION OF ABSTRACT
UNCLASSIFIED	UNCLASSIFIED	UNCLASSIFIED	SAME AS REPORT

NSN 7540-01-280-5500

91-01717

Standard form 298

21a NAME OF RESPONSIBLE INDIVIDUAL	21b TELEPHONE *(include Area Code)*	21c OFFICE SYMBOL
S. I. Chou	(619) 553–2541	Code 761

Eigenvalues Of Covariance Matrix For Two-Source Array processing

S.I. Chou
NAVAL OCEAN SYSTEMS CENTER
SAN DIEGO, CA 92152-5000

Abstract

Eigenvalue weighting appears in some noise subspace methods, in parametric signal subspace fitting methods, and in nonparametric subspace adaptive nulling beamforming. For a two-source array processing scenario, normalized eigenvalues' expressions λ_1 and λ_2 are reduced to forms depending only on a real triplet: phase-dependent variable ξ, phase-independent variable η, and power ratio $\frac{\pi_1}{\pi_2}$. (ξ, η) is confined to an isosceles-like region. We characterize

- this isosceles-like region and the many-to-one mapping from the Cartesian product of the temporal and spatial correlation unit-disks onto this region, and
- the behavior of the eigenvalues and their ratio as functions of the real triplet both analytically and graphically with respect to array processing.

1. Introduction

In this paper, we discuss some stress measure to array processing algorithms applied to scenarios with two sources. The word "stress" for a scenario is used to indicate the difficulty that an algorithm has in determining the direction of arrival of each of the two sources. Schmidt's dissertation [1] qualitatively pointed out three stressing factors to an array processing algorithm:

1. For small or medium-sized sensor arrays, the resolution is not sufficiently high so we can have unresolved arrivals.
2. Furthermore, high or 100% source correlation such as from multipaths will cause ill-conditioning or rank deficiency of the noise-free data covariance matrix.
3. The other stress factor to a direction-finding algorithm or scenario is the strength ratio between the two signals.

Here, we use eigenvalue ratios to quantitatively combine the three stressing factors. Eigenvalues in weighting expressions appear in three categories of array processing algorithms:

- in noise subspace methods [2,3,4],
- in parametric signal subspace fitting methods [4,5,6,7, 8,9,10] or its associated nonparametric subspace beamforming [11], and
- in nonparametric subspace adaptive nulling beamforming [12,13].

Only [2] is about weighted noise-eigenvectors with weights involving the corresponding noise eigenvalues. See the recent result on this in [3]. All others use weighted signal eigenvectors with weights involving the corresponding signal eigenvalues.

We give special treatment for equal power arrivals because of its many unique characteristics and its importance in real applications.

The analytical treatment begins by reviewing the expressions of the noise-free eigenvalues of the quadratic characteristic equations of the non-Hermitian product of the temporal and spatial correlation matrix given in Hudson's text[14, pp. 52-55]. The eigenvalues are normalized with respect to the product of the number of sensors and the sensor level power of the weaker source π_2, i.e., $\pi_1 \geq \pi_2$. The normalized large and small eigenvalues expressions λ_1 and λ_2 are reduced to forms depending only on the real triplet $(\xi, \eta, \frac{\pi_1}{\pi_2})$. Here, $\frac{\pi_1}{\pi_2}$ is the power ratio between the strong to weak sources at the sensor level. The real pair (ξ, η) are defined in terms of the normalized temporal and spatial coefficients ρ and ϕ respectively with each constrained to a unit-disk through

$$\eta = (1 - |\phi|^2)(1 - |\rho|^2),$$

$$\xi = \mathrm{Re}(\rho\phi^*) = |\rho||\phi|\cos(\arg\rho - \arg\phi).$$

Using our notation, the normalized eigenvalues assume the following form

$$\begin{pmatrix} \lambda_1 \\ \lambda_2 \end{pmatrix} = \frac{1}{2}\left[\frac{\pi_1}{\pi_2} + 1 + (\frac{\pi_1}{\pi_2})^{\frac{1}{2}} 2\xi\right] \times \left[1 \pm \sqrt{1 - \frac{4(\frac{\pi_1}{\pi_2})\eta}{\left[\frac{\pi_1}{\pi_2} + 1 + (\frac{\pi_1}{\pi_2})^{\frac{1}{2}} 2\xi\right]^2}}\right].$$

Before finishing the introduction of symbols and definitions, we point out the importance of the sensor coordinate origin. When two arrivals are 100% correlated, the phase difference between the two-source signals plays an important role. The specification of this variable depends on the choice of the coordinate origin. Frequently, performance such as the Cramer-Rao Lower Bound (CRLB) is plotted against this variable. If two different origins are used, the same results can be seen differently but are equivalent with a horizontal shift and possibly with the help of 2π-modulo wrap-around. Naturally, the covariance matrix and their eigenvalues are not dependent on the choice of the origin, but the expressions for the phase angles of both the steering vectors and complex source amplitudes of the signals are.

In the special case of plane waves, an array is called pairwise symmetric or inverse symmetric [15] if for each sensor located away from the origin at position coordinates (x_i, y_i, z_i) there is also a sensor located at $(-x_i, -y_i, -z_i)$. The inner product of two steering vectors for plane waves impinging onto pairwise symmetric arrays is real. For such case, the usual two-dimensional unit-disk associated with spatial correlation ϕ degenerates into a one-dimensional one.

To appear in Conference Record of the 24th Asilomar Conference on Signals, Systems and Computers, Nov 5-7, 1990, Pacific Grove, CA.

91 6 11 005

Then, the angle difference between the temporal and spatial correlation coefficients is reduced to the temporal phase difference between the two arrivals measured at the origin of the symmetric array. While the discussions of eigenvalues in this report are applicable to generic steering vectors, we call η the phase-independent variable and ξ the phase-dependent variable for convenience even though such names were motivated by the special case of plane waves impinging onto pairwise symmetric arrays.

2. An Isosceles Right-Triangle-Like Region

The phase-independent variable η depends only on the magnitude of ρ and ϕ. The phase-dependent variable ξ depends also on the angular positions of ρ and ϕ. The mapping from the complex pair (ρ, ϕ) to the real pair (ξ, η) is many to one. The range of this mapping is an isosceles right-triangle-like region bounded on its left and right by two symmetric parabolas, $\eta = (\xi \pm 1)^2$, and down below by a straight baseline, $\eta = 0$. We note the zero slope of each parabola where it meets the straight line and the 90° angle that the two parabolas intersect each other. We characterize this region with respect to the temporal and spatial correlation coefficients of array processing scenarios in Figures 1 and 2.

We will see later that among the three parameters $(\xi, \eta, \pi_1/\pi_2)$ appearing in the eigenvalues' expressions, η is the most important one. In the following, we use Figure 1 to characterize the many-to-one mapping from the Cartesian product of the two unit-disks onto the isosceles-like region with respect to η. We note that for given η, $\max(|\rho|, |\phi|) = \sqrt{1 - \sqrt{\eta}}$. Therefore, the apex point $(0, 1)$ corresponding to $\eta = 1$ can only come from the two centers of the unit-disks, i.e., $\rho = \phi = 0$. As η decreases from 1 to 0, i.e., we move from the apex towards the baseline, we shade the part of the Cartesian product of the two unit-disks mapped into the correspondingly shaded area of the isosceles-like region. Therefore, as the shaded area of the isosceles-like region expands from the apex towards the baseline, the shaded areas of the two unit-disks expand from the centers toward the unit circumferences.

When we move one-fourth of the way toward the baseline, i.e., $\eta \geq 0.75$, we find $\max(|\rho|, |\phi|) = \sqrt{1 - \sqrt{0.75}} \approx 0.36$. For two uncorrelated plane wave arrivals impinging on a uniform linear array, the first sidelobe peak has a height of $|\phi| \approx \sqrt{0.05} \approx 0.22$. At $\eta = 0.75$, the two interferers are already within a beamwidth of each other. Let us shade the corresponding range and domain of this many-to-one mapping using 45° hatching lines for this $\eta \geq 0.75$ region.

Similarly, when we have moved halfway toward the baseline in the isosceles-like region $\eta \geq 0.50$, we find $\max(|\rho|, |\phi|) = \sqrt{1 - \sqrt{0.5}} \approx \sqrt{0.3} \approx 0.54$. Let us overlay onto the earlier picture by shading the corresponding range and domain using offset 45° hatching lines for this $\eta \geq 0.50$ value. We note that the previously 45° hatched region are double-hatched now. For any point in the incremental area of the isosceles-like region corresponding to the singly 45° hatched but not double-hatched area, i.e., $0.75 \geq \eta \geq 0.50$, at least one of the originating ρ or ϕ must be located in the correspondingly shaded incremental annulus, i.e., $0.36 \leq |\rho|$ or $|\phi| \leq 0.54$.

When we move three-fourth of the way toward the baseline, i.e., $\eta \geq 0.25$, we find $\max(|\rho|, |\phi|) = \sqrt{1 - \sqrt{0.25}} \approx 0.7$. The two interferers are now within half of the half-power beamwidth of each other.

We also note that $\eta = (1 - |\phi|^2)(1 - |\rho|^2)$ is the height of the unshaded trapezoidal-like region. We can associate $\pi^2\eta$ as the product of the areas of the two unshaded annulus regions, $\pi(1 - |\phi|^2)$ and $\pi(1 - |\rho|^2)$. As this height reduces from 1 to 0, i.e., the unshaded trapezoid decreases from the original whole isosceles all the way to the zero thickness baseline, at least one of the corresponding white annuli shrinks from the original unit-disk to a zero width ring.

When the scenario is stressful, η is small, the corresponding annuli with unit outer radius are thin. The area of the temporal correlation ρ annulus can be approximated by

$$\pi(1 - |\rho|^2) = \pi(1 + |\rho|)(1 - |\rho|) \approx 2\pi(1 - |\rho|).$$

Suppose the temporal correlation coefficient has a magnitude of 99%, then the thickness of the ρ annulus is 0.01. The area of the annulus can be approximated by $2\pi(0.01)$ by letting the mean circumference of the annulus assume the outer circumference of the unit-disk, 2π. The approximation is 99.5% accurate. If the spatial correlation coefficient has a magnitude of 90%, then the thickness of the ϕ annulus is 0.1, the area of the annulus can be approximated by $2\pi(0.1)$. The approximation accuracy is 95%. We see that a combination of the high temporal and spatial correlations yield an η of approximately $(-20 + 3) + (-10 + 3) = -24$ dB.

Next we use Figure 2 to characterize some special positions in the isosceles region. Hudson's textbook[14, pp. 52-55] presented 4 out of the 17 characterizations shown there. These 4 cases are denoted by the asterisks.

The two eigenvalues are equal if and only if what is inside the radical of the eigenvalue equation vanishes. It can be shown that for this to be true we must have $\pi_1/\pi_2 = 1$ and that ξ and η must be on the left parabola of the isosceles-like region. The common eigenvalue value they share is

$$\lambda_i(\xi, (1 + \xi)^2) = (1 + \xi) = \sqrt{\eta}.$$

3. Characterizing Eigenvalues and their Ratio

We characterize the behavior of the eigenvalues and their ratio $\frac{\lambda_1}{\lambda_2}$ as functions of the real triplet $(\xi, \eta, \frac{\pi_1}{\pi_2})$. It is useful to discuss the expressions for the eigenvalue and their ratio $\frac{\lambda_1}{\lambda_2}$ for the special cases at the apex, the baseline, and the vertical axis. But instead, we characterize the special case of equal-strength arrivals and then the general case will be touched upon only lightly at the end.

The small eigenvalue is shown to diminish qualitatively and quantitatively for two-arrival scenarios increasingly stressed with high temporal and/or spatial correlations. The special case of equal strength $\frac{\pi_1}{\pi_2} = 0$ dB arrivals, also important in low-angle radar tracking, shares many rich structures of general $\frac{\pi_1}{\pi_2}$. It has several additional unique features for signal eigenvalues' ratio $\frac{\lambda_1}{\lambda_2}$ important in array processing.

The special case of equal strength $\frac{\pi_1}{\pi_2} = 0$ dB arrivals shares the following common features of general $\frac{\pi_1}{\pi_2}$ power ratios: straight line contours for constant eigenvalue λ's in Figure 3, hyperbolic λ slices for constant phase-independent variable η's in Figure 4, parabolic λ slices for constant phase-dependent variable ξ's in Figure 5.

However, we caution that unless special effort is made in plotting results, the two displayed surfaces or curves may not always meet at the supposed places. This is because the boundary curves defining parabolas in the ξ and η plane, in general, do not pass through the grid points used in the ξ and η plane.

The plots of the same information or function, using direct scale and dB scale in the vertical axis have their individual merits. The direct-scale versions show the parabolic and hyperbolic sections as well as the straight line contours in their natural coordinates as derived from the analytical studies. Versions using the dB scale better illustrate the multiplicative dependence of the eigenvalues on some of the three independent parameters. In addition, the effect of the smallest dominant eigenvalue is relative to the threshold setting, which is frequently expressed in dB scale; the condition number can be exhibited more compactly in this way.

As η approaches 0, the small eigenvalue λ_2 and the eigenvalue ratio $\frac{\lambda_1}{\lambda_2}$ tend toward $-$ and $+\infty$ dB, respectively. Similarly, as η approaches 0 for the equi-power case, $\frac{\pi_1}{\pi_2} = 0$ dB, both the upper λ_1 and lower λ_2 hyperbolas tend toward their asymptotes intersecting at $-\infty$ dB. Since we cannot display $\pm\infty$ dB, we choose to stop at a small value of $\eta = -13$ dB, which corresponds to spatially orthogonal arrivals with temporal correlation of 97.5%, or temporally uncorrelated arrivals with a $\frac{1}{4}$ fractional beamwidth spacing for a uniform linear array.

We first display for power ratio $\frac{\pi_1}{\pi_2} = 0$ dB the slices of the two signal eigenvalues λ_1 and λ_2 in dB for constant phase-independent variable η in Figure 6, and for constant phase-dependent variable ξ in Figure 7. While the parabola sections are all translation copies of each other for given $\frac{\pi_1}{\pi_2}$ values in the direct scale coordinates, their images in the dB scale are qualitatively different because of the nonlinear nature of the logarithmic function, especially near zero, which is so important for our study. Next their ratio, which is the difference in dB of the large and small signal eigenvalues, are displayed in Figures 8 and 9.

We expect the slices of the eigenvalue ratio $\frac{\lambda_1}{\lambda_2}$ surface for all constant η, phase-independent variable, and for negative constant ξ, phase-dependent variable, to intersect the 0-dB abscissa axis. Again, they do not appear to be so only because of the coarse grid systems used in making these plots, i.e., the left boundary curve of the isosceles region does not fall on the grid points.

Mesh plots and parabolic contours for eigenvalue ratio $\frac{\lambda_1}{\lambda_2}$ are shown in Figures 10 and 11 respectively. The contours of the eigenvalue ratio $\frac{\lambda_1}{\lambda_2} = l$ form a one-parameter family of parabolas having their vertices colocated at $(\xi, \eta) = (-1, 0)$, i.e., at the lower left corner of the isosceles-like triangle and their common tangent the baseline $\eta = 0$. This family includes the left boundary of the isosceles-like triangle and the baseline. Because the contours of the eigenvalue ratio $\frac{\lambda_1}{\lambda_2} = l$ pass through the lower left corner of the isosceles-like triangle, this corner is a point of discontinuity for the eigenvalue ratio $\frac{\lambda_1}{\lambda_2}$ for the special case of equal strength $\frac{\pi_1}{\pi_2} = 0$ dB. For example, the two eigenvalues are equal over the left parabolic boundary of the isosceles right-triangle-like region. Furthermore, the two equally dominant eigenvalues go down to zero jointly so that the condition number stays as unity throughout. That is, the condition numbers are the lowest possible there. However, both eigenvalues tend to zero as η tends to zero, i.e., the baseline of the region. The limit of $\frac{\lambda_1}{\lambda_2}$ approaching from the baseline of the isosceles region is ∞, while that approaching from the left boundary curve of the isosceles region is 0.

For the equi-powered case, the destructive interference scenario point is at the left apex of the isosceles region. Both eigenvalues are zero and the eigenvalue ratio $\frac{\lambda_1}{\lambda_2}$ at this point is of the 0/0 form. This point corresponds to the total cancellation of signals at the sensor element level. The total cancellation happens not only at the center of the array but at every sensor. The two steering vectors coincide and the temporal waveforms negate each other completely. Consider two strong sources behaving this way. As the power is measured by turning off one source at a time, so the equal power are considered as high and CRLB and asymptotic results apply when noise is taken into consideration.

We focus attention to the condition number's behavior over the vertical axis $\xi = 0$ of the isosceles region. For the special case of equal strength $\frac{\pi_1}{\pi_2} = 0$ dB, there is an extra 6 dB for signal eigenvalues' ratio $\frac{\lambda_1}{\lambda_2}$ over the vertical axis $\xi = 0$ accounting for the presence of an infinite slope of λ's with respect to η at the apex for the equal-power arrival case. This is reflected in the following two approximations. When $\frac{\pi_1}{\pi_2} > 10$ dB, we have

$$\frac{\lambda_1}{\lambda_2}(\text{in dB}) \approx (\frac{\pi_1}{\pi_2})(\text{in dB}) - \eta(\text{in dB}).$$

When $\frac{\pi_1}{\pi_2} \approx 0$ dB and η is less than 0.10 (or -10 dB), we have

$$\frac{\lambda_1}{\lambda_2}(\text{in dB}) \approx -\eta(\text{in dB}) + 6.$$

See Figures 12 and 13.

The variation of signal eigenvalue ratio $\frac{\lambda_1}{\lambda_2}$ across the phase-dependent variable ξ is not significant. For the special case of equal strength $\frac{\pi_1}{\pi_2} = 0$ dB, there is a 4-time or 6 dB increase on the eigenvalue ratio $\frac{\lambda_1}{\lambda_2}$ for highly correlated equi-power arrivals both temporally and spatially from changing the phase of the source correlation or the angle difference between the two unit-disk vectors from 90° to 0°.

As power ratio $\frac{\pi_1}{\pi_2}$ increases from unit value, the variation of the large eigenvalue λ_1 is essentially along the direction of the horizontal phase-dependent variable ξ. The smaller eigenvalue λ_2 is independent of both the horizontal phase-dependent variable ξ and $\frac{\pi_1}{\pi_2}$ near the baseline for large $\frac{\pi_1}{\pi_2}$ but is a strong function of the vertical phase-independent variable η. The effect of $\frac{\pi_1}{\pi_2}$ is essentially only felt by the large eigenvalue which is not sensitive to whether the scenario's (ξ, η) coordinate is close to the baseline, i.e., whether the arrivals are correlated or close to each other as far as its order of magnitude is concerned.

We have used these results for assessment of scenarios in [16] for which this paper is a synopsis.

4. Conclusion

The main contribution of this work is a manageable presentation of a compact map showing the three functions, λ_1, λ_2, and $\frac{\lambda_1}{\lambda_2}$, over all possible scenarios. This enables one to see the relative positions among different scenarios. We also present some easy-to-remember formulas that enable one to exercise back-of-envelope assessment of scenarios.

References

[1] Schmidt, R.O., *A Signal Subspace Approach to Multiple Emitter Location and Spectral Estimation*, PhD thesis, Stanford University, Stanford, CA, Nov 1981.

[2] Johnson, D.H., and S.R. De Graaf, "Improving the Resolution of Bearing in Passive Sonar Arrays by Eigenvalue Analysis," *IEEE Trans. ASSP*, vol. ASSP-30, pp. 638-647, 1982.

[3] Stoica, P., and A. Nehorai, *MUSIC, Maximum Likelihood, and Cramer-Rao Bound: Further Results and Comparisons*, Report No. 8819, Center For Systems Science, Electrical Engineering, Yale University, Sep 1988.

[4] Stoica, P., and K.C. Sharman, "Maximum Likelihood Methods for Direction-of-Arrival Estimation," *IEEE ASSP*, vol. 38, no.7, Jul 1990.

[5] Ottersten, B., *Parametric Subspace Fitting Methods for Array Signal Processing*, PhD thesis, Stanford University, Stanford, CA, Dec 1989.

[6] Viberg, M., and B. Ottersten, "Sensor Array Processing Based on Subspace Fitting," Submitted to *ASSP*, Jan 30, 1989.

[7] Viberg, M., B. Ottersten, and T. Kailath, "Detection and Estimation in Sensor Arrays Using Weighted Subspace Fitting," Submitted to *ASSP*, Jul 21, 1989.

[8] Viberg, M., *Subspace Fitting Concepts in Sensor Array Processing*, PhD thesis, Linkoping University, Linkoping, Sweden, Oct 1989.

[9] Cadzow, J.A., "Multiple Source Location: The Signal Subspace Approach," in *Conference Record of the 23rd Asilomar Conf on Signals, Systems and Computers*, Pacific Grove, CA, Oct 30-Nov 1, 1989.

[10] Stoica, P., and A. Nehorai, "Performance Study of Conditional and Unconditional Direction-of-Arrival Estimation," *IEEE ASSP*, vol. 38, no.10, Oct 1990.

[11] Farrier, D., and L. Prosper, "A Signal Subspace Beamformer," in *Proc ICASSP 90, 1990 Intl Conf on Acoustics, Speech, and Signal Processing*, pp.2815-1818, Apr 3-6, 1990.

[12] Kirsteins, I.P., and D.W. Tufts, "Rapidly Adaptive Nulling of Interference," invited paper presented at the G.R.E.T.S.I. Conference at Juan-les Pins, France, Jun 12-16, 1989, to appear in *Lecture Notes in Control and Information Sciences*, Springer Verlag.

[13] Owsley, N.L., Enhanced Minimum Variance Beamforming, in *Underwater Acoustic Data Processing*, Ed. by Y.T. Chan, NATO ASI Series, Series E: Applied Science-vol.161, Kluwer Academic Publishers, pp.285-292, 1989.

[14] Hudson, J.E., *Adaptive Array Principles*, Peter Peregrinus Ltd., London, 1981.

[15] Cox, H., "Resolving Power And Sensitivity To Mismatch Of Optimum Array Processors," *J. Acoust. Soc. Am.*, vol. 54, no.3, pp.771-785, 1973.

[16] Chou, S.I., *Eigenvalues of Covariance Matrix for Two-Source Array Processing*, NOSC TR 1370, Naval Ocean Systems Center, San Diego, CA, Oct 1990.

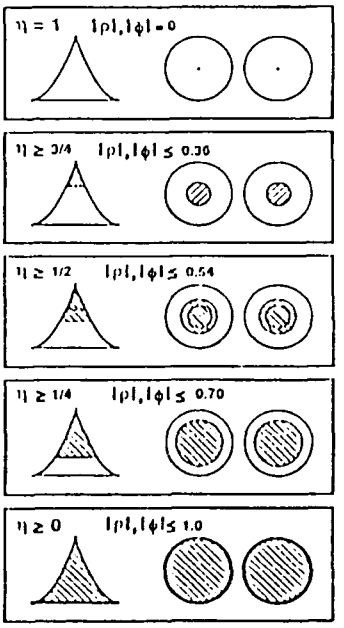

Figure 1. The many-to-one-mapping from the complex pair (ρ, φ) to real pair (ξ, η).

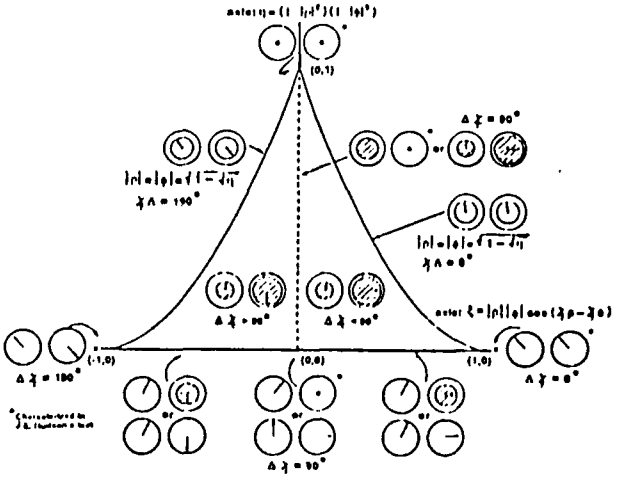

Figure 2. Mapping from cartesian product of two-unit disks to a planar region.

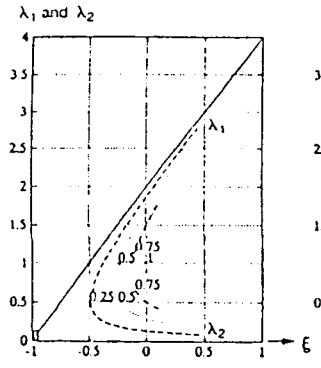

Figure 4. Hyperbolic slices: λ_1 and λ_2 vs ξ at η = 0.0, 0.25, 0.50, 0.75, 1.00 for π_1/π_2 = 0 dB.

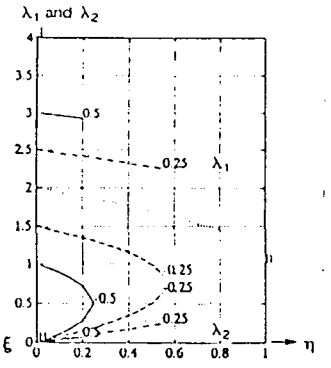

Figure 5. Parabolic slices: λ_1 and λ_2 vs η at ξ = −0.50, −0.25, 0, +0.25, +0.50 for π_1/π_2 = 0 dB.

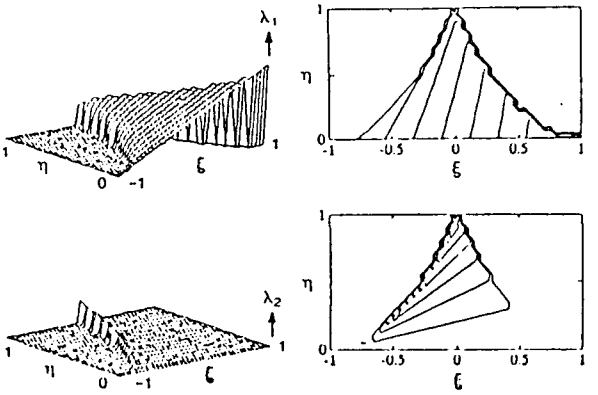

Figure 3. Mesh surfaces and straight line contours of λ_1 and λ_2 for π_1/π_2 = 0 dB.

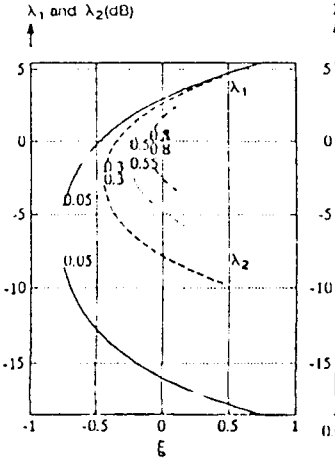

Figure 6. λ_1 and λ_2 in dB vs ξ at η = 0.05, 0.25, 0.50, 0.75, 1.00 for π_1/π_2 = 0 dB.

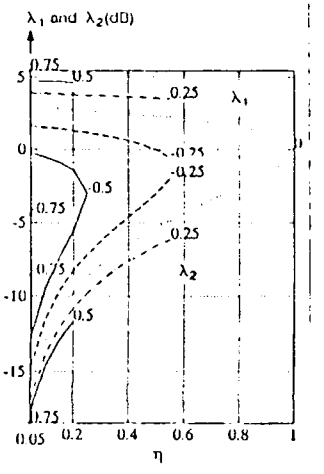

Figure 7. λ_1 and λ_2 in dB vs η at ξ = −0.5, −0.25, 0, +0.25, +0.5 for π_1/π_2 = 0 dB.

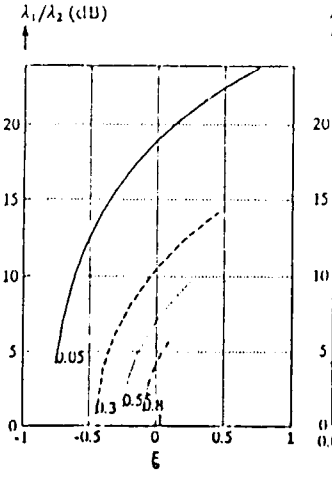

Figure 8. Slices of λ_1/λ_2 in dB at η = 0.05, 0.25, 0.50, 0.75, 1.00 for π_1/π_2 = 0 dB.

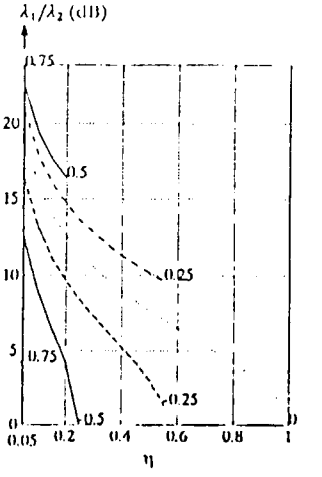

Figure 9. Slices of λ_1/λ_2 in dB at ξ = −0.05, −0.25, 0, +0.25, +0.5 for π_1/π_2 = 0 dB.

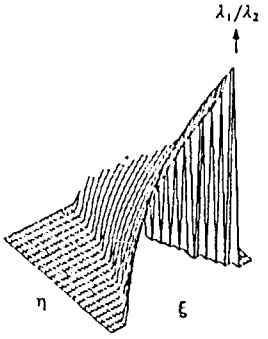

Figure 10. Mesh plot of λ_1/λ_2 in dB as function of ξ and η for π_1/π_2 = 0 dB.

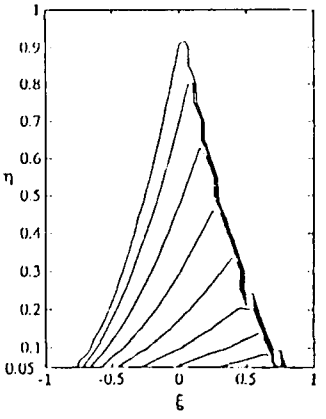

Figure 11. Parabolic contour plot of λ_1/λ_2 in dB as function of ξ and η for π_1/π_2 = 0 dB.

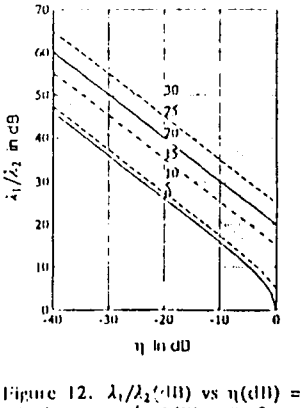

Figure 12. λ_1/λ_2(dB) vs η(dB) = −40:1:0 at π_1/π_2(dB) = 0, 5, 10, 15, 20, 25, 30 for ξ = 0.

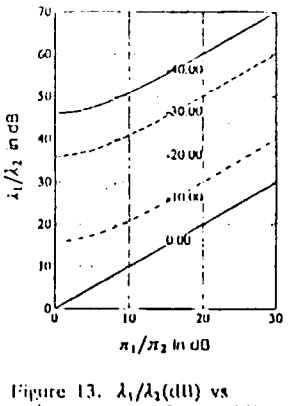

Figure 13. λ_1/λ_2(dB) vs π_1/π_2(dB) = 0:1:30 at η(dB) = −40, −30, −20, −10, 0 for ξ = 0.